pens when Kar9 with mutated phosphorylation sites associates with both SPBs and therefore with both sets of cytoplasmic microtubules? Both SPBs repeatedly attempt to align themselves along the mother-bud axis, with the net result that the spindle "dances" as each SPB tries to move toward the bud. Together, these data support the notion (*8*) of directed transport of microtubule ends by Myo2 along polarized actin cables (see the figure, steps 3 and 4).

So, it now appears that microtubules are led to the site of polarization like a "reluctant groom," rather than finding the site without help like an enlightened one. Does this behavior apply to microtubules in animal cells, where distances and microtubule dynamics are greater and there is no single attachment point (like the yeast bud) for the actin cytoskeleton? Indeed, in fibroblasts, microtubules are targeted to focal adhesions probably by associated actin stress fibers (*9*). Also, there is a striking parallel between the behavior of Kar9 and that of the animal APC (adenomatous polyposis coli) protein. It has been suggested that APC is the functional equivalent of Kar9 based on its binding to EB1 (the mammalian Bim1) and on limited sequence homology. APC moves to the ends of microtubules in a kinesin-dependent manner (*10*) and may participate in reorientation of the microtubule organizing center (*11*).

The yeast studies raise a number of interesting questions. Although Cdc28 is involved in the asymmetric loading of Kar9, how do its associated cyclins become asymmetrically loaded? Also, how are the oriented microtubules ultimately anchored in the cell cortex? One possibility is the formin protein family. In yeast, formins participate in Kar9-mediated microtubule capture by nucleating the assembly of actin cables (*12*, *13*). But in mammalian cells, formins regulate selective microtubule stabilization, binding to microtubules both in vivo and in vitro (*14*). Such cortical anchor proteins may also regulate the activity of captured microtubules to give controlled shrinkage in yeast or capping of stabilized microtubules in mammalian cells.

The new studies shift our view of how microtubule dynamics contribute to generating cellular asymmetries. They point to the guiding of microtubules by actin microfilaments through factors that initially interact separately with the two elements. The dynamics of microtubules are still likely to be important in this new view, especially because the myosin "target" is one that moves along actin cables. It will be interesting to test this model in other systems, such as migrating cells, neuronal growth cones, or polarized epithelia, where actin microfilaments and microtubules collaborate to effect cellular asymmetries.

References

1. M. Kirschner, T. Mitchison, *Cell* **45**, 329 (1986).
2. D. Liakopoulos *et al.*, *Cell* **112**, 561 (2003).
3. H. Maekawa *et al.*, *EMBO J.* **22**, 438 (2003).
4. E. Hwang *et al.*, *J. Cell Biol.* **161**, 483 (2003).
5. G. Pereira *et al.*, *EMBO J.* **20**, 6359 (2001).
6. R. K. Miller, M. D. Rose, *J. Cell Biol.* **140**, 377 (1998).
7. D. L. Beach *et al.*, *Curr. Biol.* **10**, 1497 (2000).
8. H. Yin *et al.*, *Nature* **406**, 1013 (2000).
9. I. Kaverina *et al.*, *J. Cell Biol.* **142**, 181 (1998).
10. Y. Mimori-Kiyosue *et al.*, *J. Cell Biol.* **148**, 505 (2000).
11. S. Etienne-Manneville, A. Hall, *Nature* **421**, 753 (2003).
12. M. Evangelista *et al.*, *Nature Cell Biol.* **4**, 32 (2002).
13. I. Sagot *et al.*, *Nature Cell Biol.* **4**, 42 (2002).
14. A. F. Palazzo *et al.*, *Nature Cell Biol.* **3**, 723 (2001).

OCEAN SCIENCE

Ocean Freshening, Sea Level Rising

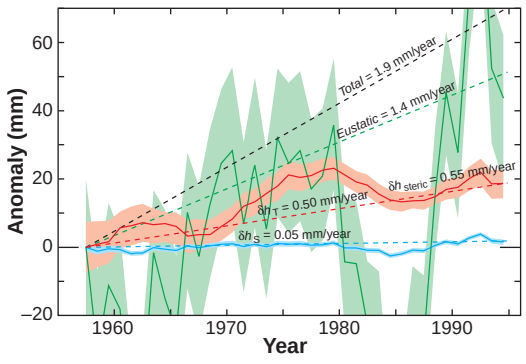
Walter Munk

The rate of the global sea level rise and its causes has been debated for a century, but no definitive conclusion has been reached. Traditional tide gage estimates are attributed to two causes: thermal expansion of warming oceans, and freshwater exports from continents. Surveys of glaciers, ice sheets, and other continental water storage can place only very broad limits of –1 to +1 mm/year on sea level rise from freshwater export. A recent survey of global ocean freshening provides an alternative estimate but raises a host of new issues.

Sea level rise played an important role in recent assessments by the Intergovernmental Panel on Climate Change (IPCC) (*1*, *2*). In their reports, the IPCC generally assumed a sea level rise in the 20th century of 1.5 to 2.0 mm/year, largely on the basis of tide gage records (*3*). The main causes of this rise are the thermal expansion and hence lower density of a warming ocean (steric rise) and the import of fresh water from continents (eustatic rise). In 1995, the IPCC concluded that "the rise in sea level has been due largely to the concurrent increase in global temperature over the last hundred years" but went on to refer to additional contributions from "melting of glaciers, ice caps and ice sheets" [(*1*), p. 363]. Thus, the 1995 IPCC report considered the rise to be primarily steric.

The situation changed radically when Levitus and co-workers (*4*, *5*) reported an increase in global ocean heat storage by 2 $\times 10^{23}$ J (equivalent to 0.44 W/m^2) in the past 50 years. This ocean warming is consistent with a steric rise of just 0.5 mm/year. The record (red curve in the first figure) is dominated by oscillations on decadal time scales, introducing large errors into estimates of century-scale trends. Nonetheless, the thermal expansion of 0.5 mm/year falls far short of the traditional estimates of 1.5 to 2.0 mm/year. The data thus suggest a dominant (rather than secondary) role for the eustatic contributions.

Yet the IPCC's "central" estimate (*2*) for the eustatic contribution is only 0.2 mm/year (although the error bars are so generous as not to preclude a substantial eustatic contribution). Further, polar melting would result in movement of water mass toward the equator, causing a decrease in the rate of Earth's rotation. In contrast, observations show a (nontidal) increase in



A large eustatic rise? Red and blue curves are the temperature-induced (δh_T) and salinity-induced (δh_S) components of the steric anomaly, $\delta h_{steric} = \delta h_T + \delta h_S$. The time series are spatially averaged (50°S to 65°N), 5-year running means computed for the upper 3000 m of the ocean. Shaded bands give standard errors; dashed lines are least-squares trends. The green curve gives the eustatic rise, calculated as 36.7 δh_S (see text). The total sea level rise from the temperature and salinity surveys (after correction for melting sea ice) is the sum of the thermosteric and the eustatic rise, $\delta h_T + 36.7\ \delta h_S = 0.5 + 1.4 = 1.9$ (mm/year). [Adapted from (*7*)]

The author is at the Scripps Institution of Oceanography, University of California, San Diego, La Jolla, CA 92093, USA. E-mail: wmunk@ucsd.edu

Earth's rotation (attributed to a movement of mass toward the poles in response to the unloading of ice mass since the last glacial maximum). Hence, the combined steric and eustatic contributions fall well short of 1.5 to 2.0 mm/year. Therein lies the enigma (*6*).

A recent survey by Antonov *et al*. (*7*) may provide some possible clues to solving the enigma. The authors showed that the mean salinity of the global ocean has decreased slightly between 1954 and 1997. Combining the increased temperature and decreased salinity, one obtains a steric sea level rise (*8*) of

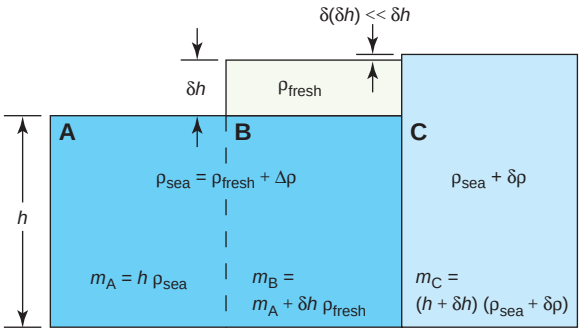
$$\delta h_{\text{steric}} = \delta h_T + \delta h_S = 0.50 + 0.05 = 0.55 \text{ (mm/year)}$$

The salinity-related steric expansion, δh_S, of 0.05 (±0.02) mm/year (blue curve in the first figure) is widely interpreted as a minor addition to thermal expansion, δh_T. But interpretation of the salinity-induced component depends on the source of the expansion. If the decrease in salinity is associated with melting of ice sheets and other changes in continental water storage, then it provides independent evidence for a dominant eustatic contribution. In any case, it must not be counted twice, once steric and once eustatic.

Here, I consider three modes of ocean freshening. First, there are regions of large freshening in which the salinity-induced and temperature-induced steric rises nearly cancel [for example, such a situation occurred in the Labrador Sea between 1960 and 1980 (*7*)]. Such events are associated with intrusions of cold, fresh waters into warm, salty waters of equal density and leave the global average salinity unchanged. Second, melting of floating ice fields may freshen the ocean without raising sea level. Third, fresh water may be imported from continents. Only this third mode leads to a global eustatic rise in sea level: $\delta h_{\text{eustatic}} = (\rho/\Delta\rho)\delta h_S$ where $\rho = 1028$ kg/m^3 is the density of seawater and $\Delta\rho = 28$ kg/m^3 is the incremental density of seawater relative to fresh water of the same temperature.

The multiplier, $\rho/\Delta\rho = 36.7$, is a consequence of conservation of mass (see the second figure). Its large value is perhaps surprising, but can be made plausible by the following consideration. Adding a layer δh of fresh water to fresh water ($\Delta\rho = 0$) raises the level without decreasing salinity. Clearly, the density perturbation $\delta\rho$ must be proportional to the salinity ($\Delta\rho$), $\delta\rho = -\Delta\rho(\delta h/h)$, which is consistent with $\delta h_{\text{eustatic}} = (\rho/\Delta\rho)\delta h_S$.

The salinity-induced steric sea level rise $\delta h_S = 0.05 \pm 0.02$ mm/year then yields a eustatic rise of $36.7\ \delta h_S = 1.8$ (±0.7) mm/year. A eustatic rise of 1.8 mm/year over an ocean area of 3.6×10^8 km^2 would require a melt volume of 650 (±250) km^3/year. Antonov *et al*. obtained a value of 471 km^3/year following a somewhat different argument (*7*). These are, however, upper limits because of contributions to the freshening of the ocean from melting sea ice.



Freshening the ocean. The unperturbed ocean (**A**) has a depth h and a density $\rho_{sea} = \rho_{fresh} + \Delta\rho = 1000 + 28 = 1028$ (kg/m^3). Continental runoff adds a layer δh of density ρ_{fresh} (**B**). Thorough mixing of this layer with the underlying ocean (**C**) results in a perturbation $\delta\rho$ (a negative quantity) relative to the initial density. The additional change in depth, $\delta(\delta h)$, due to mixing is negligible. Equating the total water masses before and after mixing, $m_B = m_C$, yields a eustatic sea level rise $\delta h_{\text{eustatic}} = -h(\delta\rho/\Delta\rho)$. The steric rise $\delta h_{\text{steric}} = -\int dz\ \delta\rho/\rho = -h(\delta\rho/\rho)$, and accordingly $\delta h_{\text{eustatic}} = (\rho/\Delta\rho)\delta h_{\text{steric}} = 36.7\ \delta h_{\text{steric}}$.

Sea ice covers an area of ~10^7 km^2 (with ±30% seasonal departures) at a thickness of ~3 m (*9, 10*). The total sea ice volume is thus 30,000 km^3. Shrinking of the ice-covered area reduces the volume by 0.3% or 90 km^3 per year. There is, however, no consensus on the rate of sea ice thinning. Johannessen *et al.* (*10*) place their confidence in the measurements by Nagurnyi *et al.* (*11*) of the dispersion of elastic-gravity waves in the floating ice cover. These waves are generated by ocean swell and propagate hundreds to thousands of kilometers into the ice sheet; their dispersion is sensitive to ice thickness. From these data, Johannessen *et al.* deduce a thinning by only 4% over the past 20 years. This thinning is equivalent to a loss of 60 km^3/year, yielding a total loss of sea ice from shrinking and thinning of 150 km^3/year.

This annual loss is equivalent to about 135 km^3 of fresh water, which must be subtracted from the above estimate of the eustatic sea level rise (650 km^3/year). Hence, the eustatic rise corresponds to 515 km^3/year, or 1.4 mm/year (green curve in the first figure). Adding this eustatic rise to the steric rise of 0.5 mm/year, we end up with an estimated 1.9 mm/year for the total sea level rise—near the upper limit of the traditional estimates of 1.5 to 2.0 mm/year.

I do not propose that this is the solution to the enigma. Cabanes *et al.* (*12*) have presented evidence for a bias in the location of the tide gages, favoring regions of abnormal thermal expansion. They argue for a 20th-century mean rate of 0.5 mm/year dominated by thermal expansion. Miller and Douglas (*13*) have reanalyzed the same basic data set in large ocean regions and come up with a traditional estimate of global sea level rise dominated by the eustatic contribution. The jury is still out on the interpretation of the tide gage records.

With regard to the thinning of sea ice, submarine transects with upward-looking sonars indicate a much higher rate of thinning by 1.5 m over the past 20 years (*9*). Some of this thinning may result from changes in ice distribution caused by changes in wind stress over the Arctic. The sonar data give 600 to 800 km^3 of fresh water per year—more than enough to account for the entire freshening. This would leave no room for a eustatic contribution (consistent with Cabanes *et al.*) and would suggest a continental water import (*14*) that is in line with the lower limits of the IPCC assessment.

The large discrepancy between the sea ice thinning estimates from the sonar method and the wave method leaves the interpretation of freshening in limbo. As mentioned above, the global ocean heat storage has increased by 2×10^{23} J in the past 50 years, or 4×10^{21} J/year on average (*4, 5*). A proportional increase over the arctic sea ice area would melt 400 km^3/year. But we must allow for the larger than average increase in radiation at high latitudes and the effective albedo of the floating ice sheet. The two effects might just cancel; in any event, these considerations suggest a substantial contribution to ocean freshening from melting sea ice.

The future is another story. Global coverage by satellite altimetry (which is replacing tidal estimates) shows a notably larger than average level rise in the last decade of the century (*15*). The detection of the relatively slow century-scale trend is plagued by the dominance of high (decadal) frequencies in the spectrum of the rate of sea level variability. It will take several decades to obtain good estimates of the role of global warming in sea level rise.

In the meantime, 20th-century sea level remains an enigma—we do not know whether warming or melting was dominant, and the budget is far from closed. Ocean freshening, despite large error bars, places some welcome independent constraints on sea level rise and will hopefully be the focus of further research.

References and Notes

1. IPCC, *Climate Change 1995: The Science of Climate Change*, J. T. Houghton *et al.*, Eds. (Cambridge Univ. Press, New York, 1995).
2. IPCC, *Climate Change 2001: The Scientific Basis*, J. T. Houghton *et al.*, Eds. (Cambridge Univ. Press, New York, 2001).
3. B. C. Douglas, M. S. Kearney, S. P. Leatherman, *Sea Level Rise: History and Consequences* (Academic Press, New York, 2001).
4. S. Levitus, J. I. Antonov, T. P. Boyer, C. Stephens, *Science* **287**, 2225 (2000).
5. S. Levitus *et al.*, *Science* **292**, 267 (2001).
6. W. Munk, *Proc. Natl. Acad. Sci. U.S.A.* **99**, 6550 (2002).
7. J. I. Antonov, S. Levitus, T. P. Boyer, *J. Geophys. Res.* **107**(C12), 14-1 (2002).
8. Steric sea level is defined by $\delta h_{steric} = -\int dz\, \delta\rho/\rho$, with $\delta\rho/\rho = -\alpha\delta_T + \beta\delta_S$ giving the temperature-induced and salinity-induced contributions, δh_T and δh_S, respectively. The coefficient of thermal expansion, α, is a sensitive function of the temperature $T(z)$, but not as sensitive as it is for fresh water. With salinity and pressure taken into account, α remains within 10% of 1.8×10^{-4} °C^{-1} for climate-related warming. The salinity coefficient β varies from 0.82 psu^{-1} at 0°C to 0.79 psu^{-1} at 10°C.
9. P. Wadhams, *Ice in the Ocean* (Gordon and Breach, Sydney, 2000).
10. O. M. Johannessen *et al.*, *Arctic Climate Change—Observed and Modeled Temperature and Sea Ice*, Nansen Technical Report 218 (Bergen, Norway, 2003).
11. A. P. Nagurnyi, V. G. Korostelev, V. V. Ivanov, *Meteor. Hydrol.* **3**, 72 (1999).
12. C. Cabanes, A. Cazenave, C. Le Provost, *Science* **294**, 840 (2001).
13. L. Miller, B. D. Douglas, paper presented at the EGS-AGU-EUG joint assembly, Nice, France, 6 to 11 April 2003.
14. D. P. Chambers, J. Chen, R. S. Nerem, B. D. Tapley, *Geophys. Res. Lett.* **27**, 3073 (2000).
15. A. Cazenave, paper presented at *WOCE and Beyond*, San Antonio, TX, 21 November 2002 (www.woce2002.tamu.edu/cazenave.ppt).

16. I thank C. Wunsch, C. J. R. Garrett, J. Antonov, T. Barnett, J. Gregory, D. Pierce, P. Wadhams, and P. Woodworth for helpful suggestions. The author holds the Secretary of the Navy Chair in Oceanography.

PLANETARY SCIENCE

The Surface of Mars: Not Just Dust and Rocks

Matthew P. Golombek

The spectacular results from the Thermal Emission Imaging System (THEMIS) reported by Christensen *et al.* on page 2056 of this issue (*1*) resolve a long-simmering uncertainty about the value of thermal infrared measurements for understanding the bedrock geology of Mars.

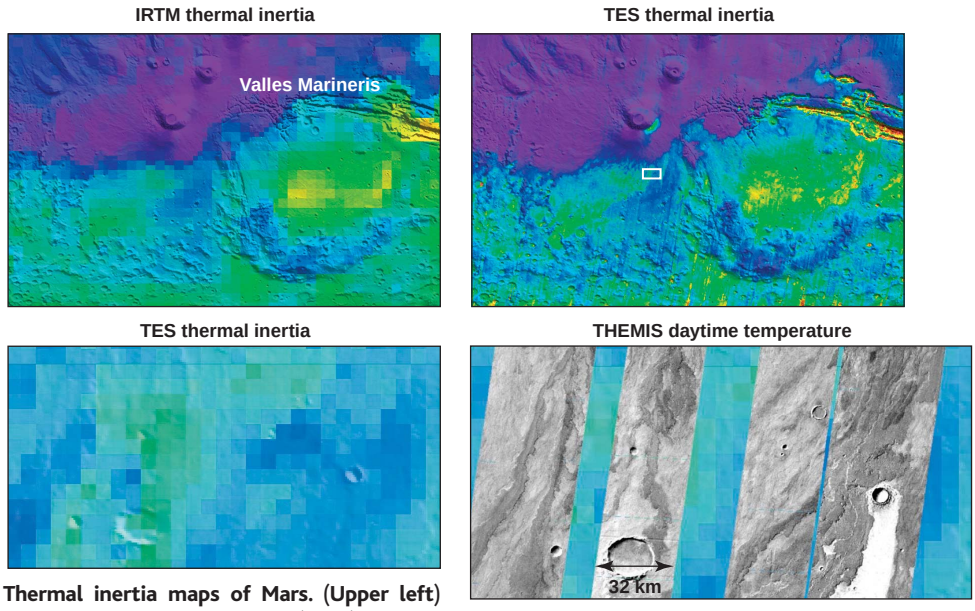
Ever since the Viking orbiter returned thermal infrared measurements at roughly 1° (60 km) resolution (*2*), scientists have argued about the utility of the resulting thermal inertia maps for identifying the bedrock geology, which is essential for deciphering the geologic history of Mars. Thermal inertia is a measure of the rate at which surface materials change temperature. It can be related to particle size and cohesion, such that large particles and cemented, fine-grained materials have higher thermal inertias than small particles or loosely bound, fine-grained materials (see the figure).

The Viking infrared measurements showed broad areas with very low thermal inertia, indicative of surfaces dominated by very fine-grained, loosely bound dust. In other areas, up to a third of the surfaces are covered by individual rocks larger than 0.1 m in diameter, as seen at the Viking 1, Viking 2, and Mars Pathfinder landing sites (*3*, *4*). Because no outcrop or bare rock was evident at spatial scales of 60 km, thermal inertia and albedo have been used to map a "surface layer" on Mars related to eolian (wind) processes.

However, mapping eolian surface materials has little obvious relevance to the underlying bedrock geology, which has been typically inferred from surface morphology at scales of 1 km in Viking visible images. Thermal inertia data from Mars Global Surveyor Thermal Emission Spectrometer (TES) at a scale of 3 km/pixel showed an improved spatial relationship with inferred bedrock geology, but still did not offer fundamentally new insights into the underlying rock units (*5*).

THEMIS data have forever changed the way geologists look at the surface of Mars. At a spatial scale of 100 m/pixel, thermal images of Mars show a large range in temperatures that allow the bedrock geology and the physical nature of the surfaces to be inferred directly (*1*). Certain areas have such high thermal inertia that they must be exposed bedrock. Other areas show differences in surface temperature that allow direct inference of particle sizes on the surface. These differences allow the definition of distinct contiguous geologic units that can be observed directly in the images.

Mars still exhibits areas that are covered by thick deposits of fine-grained, loosely bound dust. But other areas show a rich di-



Thermal inertia maps of Mars. (Upper left) Viking infrared thermal mapper (IRTM) thermal inertia map, overlain on a Viking visible mosaic of a portion of the western hemisphere of Mars (10°N to 50°S and 200°E to 300°E). IRTM pixels (*6*) are 2° by 2° (120 km). Thermal inertia is low (purple, 40 J m^{-2} s$^{-0.5}$ K^{-1}) over Tharsis and high (yellow, 400 J m^{-2} s$^{-0.5}$ K^{-1}) along Valles Marineris. (**Upper right**) Higher resolution (1/8° by 1/8°) TES thermal inertia (*4*) overlain on a Viking visible mosaic of the same area. TES shows greater variation in thermal inertia than IRTM, from 40 (purple) to 500 J m^{-2} s$^{-0.5}$ K^{-1} (red). Neither shows much relationship to the underlying morphology. (**Lower left**) Close up of the white box in the upper right, showing the TES thermal inertia from 250 (blue) to 325 J m^{-2} s$^{-0.5}$ K^{-1} (green). The area shown is 225 km by 105 km. (**Lower right**) Daytime THEMIS thermal image at 100 m/pixel resolution, overlain on TES thermal inertia. The image shows multiple lava flows, with details of the flow morphologies and drastically different physical properties. Dark areas are cooler during the day with higher thermal inertia and therefore rockier; bright areas are warmer during the day with lower thermal inertia and thus dustier.

CREDIT: NASA

The author is in the Jet Propulsion Laboratory, California Institute of Technology, Pasadena, CA 91109, USA. E-mail: mgolombek@jpl.nasa.gov